CrossMark

Crystal growth and characterization of semi-organic 2-amino-5-nitropyridinium bromide (2A5NPBr) single crystals for third-order nonlinear optical (NLO) applications

Sivasubramani Vediyappan[1] · Raja Arumugam[1] · Karuppasamy Pichan[1] · Ramachandran Kasthuri[1] · Senthil Pandian Muthu[1] · Ramasamy Perumal[1]

Abstract

Semi-organic nonlinear optical (NLO) 2-amino-5-nitropyridinium bromide (2A5NPBr) single crystals have been grown by slow evaporation solution technique (SEST) with the growth period of 60 days. The single-crystal XRD analysis confirms the unit cell parameters of the grown crystal. The crystallinity of grown 2A5NPBr was analyzed by powder X-ray diffraction (PXRD) measurement. The presence of functional groups of 2A5NPBr crystal was confirmed by Fourier transform infrared (FTIR) spectrum analysis. The optical transmittance of the grown crystal was analyzed by UV–Vis–NIR analysis. It shows good transparency in the visible and NIR region and it is favorable for nonlinear optical (NLO) device applications. The chemical etching study was carried out and it reveals that the grown crystal has less dislocation density. The photoconductivity study reveals that the grown crystal possesses positive photoconductive nature. The thermal stability of the crystal has been investigated by thermogravimetric (TG) and differential thermal analysis (DTA). The dielectric constant and dielectric loss as a function of frequency were measured. The electronic polarizability (α) of 2A5NPBr molecule has been calculated theoretically by different ways such as Penn analysis, Clausius–Mossotti relation, Lorentz–Lorenz equation, optical bandgap, and coupled dipole method (CDM). The obtained values of electronic polarizability (α) are in good agreement with each other. Laser damage threshold (LDT) of 2A5NPBr crystal has been measured using Nd:YAG laser with the wavelength of 1064 nm. Third-order nonlinear optical property of the grown crystal was studied by Z-scan technique using He–Ne laser of wavelength 632.8 nm.

1 Introduction

In the recent days, there is need for good quality single crystals with sufficiently large nonlinear optical responses that can be used for applications such as telecommunications, optical data storage, optical switching, optical modulation, photodynamic therapies, and so on [1, 2]. Most of the organic single crystals possess large NLO property but poor physical properties such as optical, mechanical, thermal, and laser damage threshold. The inorganic materials have excellent physical properties but moderate NLO efficiency. Organic and inorganic materials are combined to make new semi-organic crystals for nonlinear optical (NLO) device

applications. 2-amino-5-nitropyridine (2A5NP) is a good organic NLO material and the crystal structure was studied by Aakeroy et al. [3]. It has an interesting molecular structure where nitro group acts as electron acceptor and the amino group acts as electron donor. The aromatic pyridine ring acts as a cationic bonding site, the nitrogen as a proton acceptor and the amino group acts as a proton acceptor [4]. The 2A5NP derivative crystals have attracted attention due to their large nonlinear response with improved optical, thermal, laser damage threshold, and mechanical stabilities. The large NLO effect and good physico-chemical properties are due to the presence of π-conjugated electronic system with active short/multiple hydrogen bonding and Coulomb interaction between 2A5NP cation and involved counter anions. In addition, the density of the chromophores (NO_2, NH_2 and NH^+) and herringbone arrangements are also responsible for the enhancement of NLO effect. 2A5NP derivative crystals, namely, 2-amino-5-nitropyridinium p-phenolsulfonate (2A5NPP) and 2-amino-5-nitropyridinium

✉ Sivasubramani Vediyappan
sivasubramaniv1989@gmail.com

1   SSN Research Centre, SSN College of Engineering, Chennai, Tamilnadu 603 110, India

p-toluenesulfonate (2A5NPT), exhibit larger NLO efficiency compared to KDP material [4, 5]. A detailed literature survey shows that 2A5NP family single crystals can be used for SHG device applications. However, the third harmonic generation crystals can also be used in optical limiting, photonics, and optoelectronics device applications [6]. It will be more interesting if the second-order and third-order NLO properties are both well possessed by one compound [7]. The grown crystal exhibits polymorphic structure (different crystal structures with the same molecule) with two different crystal structures such as centro ($P2_{1/a}$) and noncentrosymmetric ($P2_1$) space groups. The crystal structures were already studied by Pecaut et al. [8] and the crystal growth and its preliminary characterizations were reported [9, 10]. The present work has been taken up with the aim of growing good quality semi-organic single crystals of 2-amino-5-nitropyridinium bromide (2A5NPBr) for third-order nonlinear optical (NLO) device applications.

The present article describes growth of 2A5NPBr single crystal by slow evaporation solution technique and its characterizations such as single-crystal XRD (SXRD), powder XRD (PXRD), Fourier transform infrared spectrum (FTIR), UV–Vis–NIR, chemical etching, thermogravimetric (TG) and differential thermal analysis (DTA), photoconductivity, dielectrics, electronic polarizability, laser damage threshold (LDT), and third-order nonlinear optical studies.

2 Experimental procedures

2.1 Material synthesis and crystal growth

2-amino-5-nitropyridine is a weak Bronsted base and it acquires a proton from strong or medium acids with pH < 2 [5]. The high purity of 2-amino-5-nitropyridine (Alfa Aesar)

and hydrogen bromide (Merck) reagents was taken in the molar ratio of 1:2 with Millipore water ($\rho = 18.2$ MΩ cm) as a solvent. The reactant containing solution has been continuously stirred for 5 h using the magnetic stirrer. The reaction scheme of 2A5NPBr is shown in Fig. 1. The homogeneous solution was allowed to dry by heating to an optimized temperature 50 °C. The synthesized material was further purified by acetone. The growth of 2A5NPBr was performed by Millipore water with the pH of 1.7. The purity of the title material was further improved by recrystallization process (3 times). The good quality 2A5NPBr single crystals were successfully grown by slow evaporation solution technique (SEST) in the period of 60 days. The photographs of as-grown and cut and polished crystal wafers are shown in Fig. 2a, b, respectively. Already, 2A5NPBr material has been synthesized and single crystals have been grown by three different research groups [8–10]. The grown crystal exhibits polymorphic crystal structure [centro ($P2_{1/a}$) and noncentrosymmetric ($P2_1$) phase]. So far, the precise conditions for the crystallization of each phase (by varying the growth conditions such as solvent, temperature, and pH) have not been determined [10]. Dhanushkodi et al. have grown noncentrosymmetric phase single crystal in the pH value of 2.04 [9]. In the present work, the centrosymmetric phase single crystal has been grown in the pH value of 1.7. The pH value of solution may possibly be the reason for different crystal structures. The growth conditions have to be optimized for better understanding of two different crystal structures of 2A5NPBr.

Fig. 1 Reaction scheme of 2A5NPBr
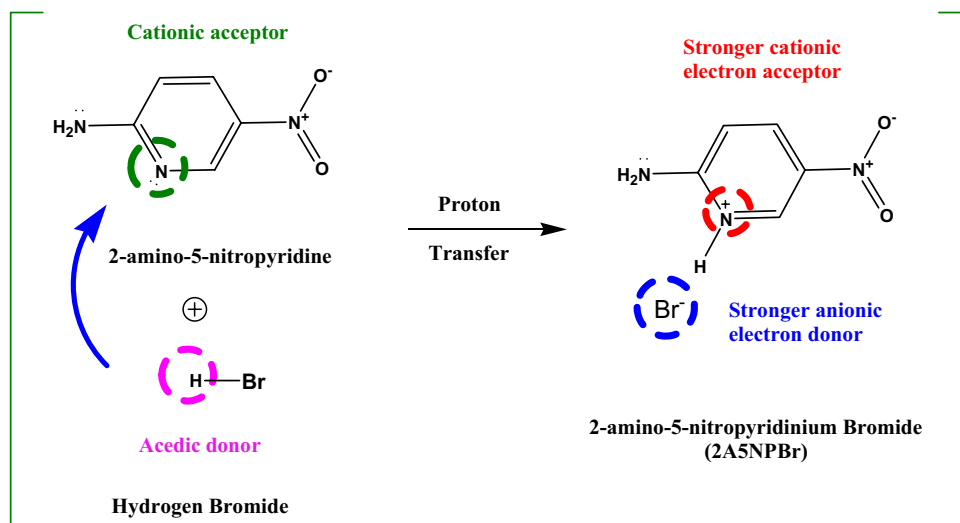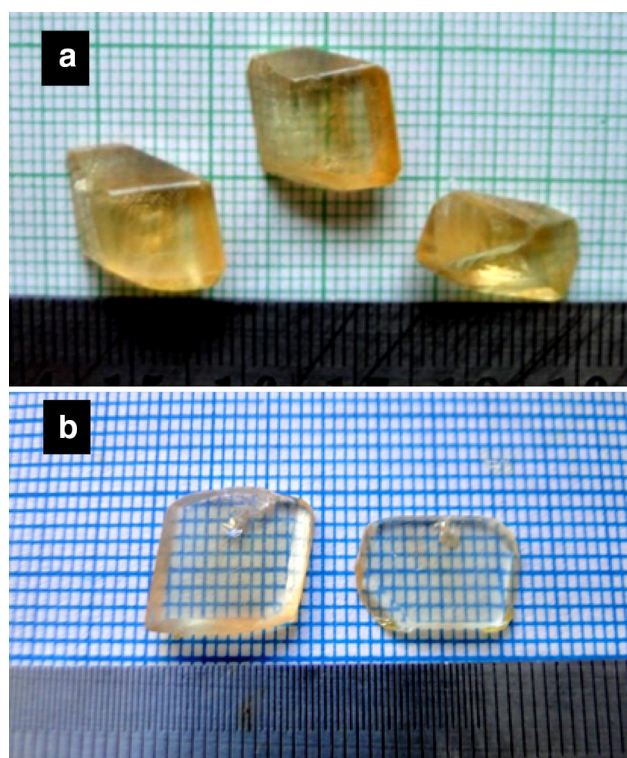
Fig. 2 **a** As grown 2A5NPBr single crystal and **b** cut and polished 2A5NPBr crystal wafers

3 Characterization analysis

3.1 X-ray diffraction analysis

The unit cell dimension of the grown crystal was confirmed by single-crystal X-ray diffraction analysis (SXRD) using Enraf Nonius CAD-4 diffractometer with graphite monochromated MoK_α ($\lambda = 0.710$ Å) radiation. The result shows that the grown crystal belongs to monoclinic crystal system with the space group $P2_{1/a}$. The obtained unit cell parameter values agree well with previously reported values [8] and it is given in Table 1.

The crystal morphology of the title crystal was generated by the WinXMorph software program [11]. The single-crystal XRD data were used as input to generate the morphology of the grown crystal. The indexed morphology of 2A5NPBr single crystal is shown in Fig. 3. The good quality 2A5NPBr crystals were crushed into fine powder and it was subjected to powder XRD (PXRD) analysis using XPERT-PRO X-ray diffractometer with $CuK_{\alpha 1}$ radiation ($\lambda = 1.5418$ Å) at room temperature. The PXRD analysis was performed in the 2θ scanning range from $10°$ to $60°$ and the obtained peaks have been indexed by the TWO THETA software. The parameters obtained from PXRD of 2A5NPBr are shown in Table 2. The obtained PXRD pattern is shown in Fig. 4. The well-defined sharp peaks at specific 2θ angles reveal the high degree of crystallinity in the title material.

3.2 FTIR spectral analysis

Fourier transform infrared (FTIR) spectral analysis was used to find the various types of functional groups in the grown crystal. In the present case, FTIR spectrum was recorded in the range between 400 and 4000 cm^{-1} using Bruker AXS FTIR spectrometer with KBr pellet technique at room temperature. Figure 5 shows the FTIR spectrum of 2A5NPBr compound. The absorption band observed at 3324 cm^{-1} is due to the presence of NH_2 asymmetric stretching vibration. The NO_2 symmetric and asymmetric stretching vibrations were observed at 1520 and 1345 cm^{-1}, respectively [9]. The peak at 1665 cm^{-1} is due to aromatic asymmetric stretching vibration of C=N group. The absorption peak at 1615 cm^{-1} is due to the presence of N–H bending vibration. The C–H in-plane bending and C–H out-of-plane bending occur at

Table 1 Single-crystal XRD data for 2A5NPBr crystal

Molecular formula		$C_5H_6O_2N_3Br$
Molecular weight		220.03 g/mol
Density		1.887 g/cm^3
Space group		$P2_{1/a}$
Crystal system		Monoclinic
Unit cell parameters	Reference [8]	Present work
a (Å)	12.686 (± 2)	12.62 (± 0.018)
b (Å)	7.819 (± 9)	7.80 (± 0.011)
c (Å)	7.846 (± 9)	7.82 (± 0.012)
α	90 0.00°	90.00°
β	91.14° (± 1)	91.24 (± 0.03)°
γ	90.00°	90.00°
Volume (Å^3)	778 (± 1)	770 (± 3)

Fig. 3 Morphology of 2A5NPBr single crystal

Fig. 4 Powder X-ray diffraction spectrum for 2A5NPBr single crystal

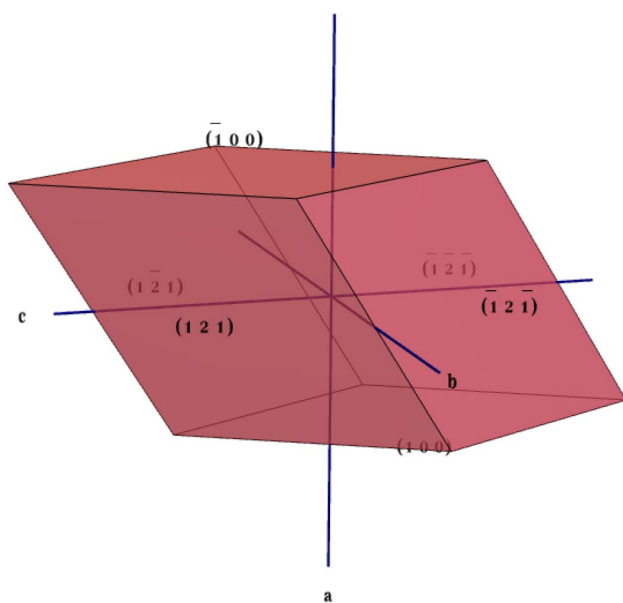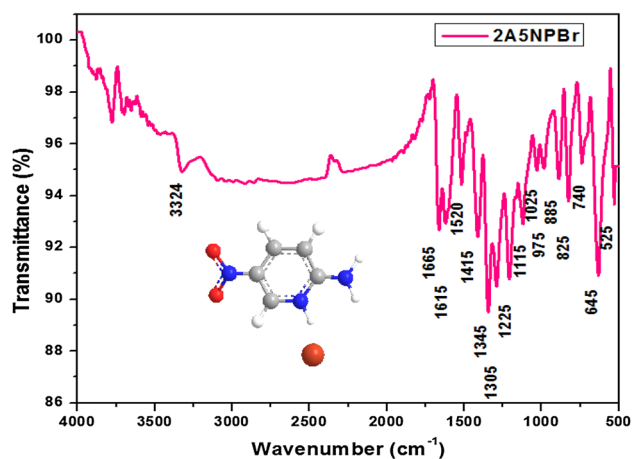Fig. 5 FTIR spectrum of 2A5NPBr material

Table 2 Calculated values from the powder X-ray diffraction analysis

2 theta position (°)	Peak height (counts)	FWHM	d-spacing (Å)	Relative intensity (%)
12.2878	112.62	0.1476	7.20328	11.79
13.1171	138.29	0.1476	6.74968	14.48
16.4218	123.68	0.1476	5.39806	12.95
18.5487	166.91	0.1476	4.78361	17.48
20.9775	231.15	0.1476	4.23494	24.20
22.8778	244.31	0.1968	3.88728	25.58
23.8500	452.14	0.1476	3.73099	47.35
24.8787	112.23	0.1476	3.57900	11.75
25.8177	430.60	0.0984	3.45091	45.09
26.1314	766.05	0.1476	3.41020	80.22
27.4225	954.97	0.1968	3.25250	100.00
27.9384	273.75	0.1476	3.19360	28.67
30.2446	553.16	0.1476	2.95514	57.92
33.0649	80.23	0.1476	2.70924	8.40
34.0566	77.08	0.2952	2.63259	8.07
35.1990	41.94	0.3936	2.54972	4.39
37.8131	80.89	0.1968	2.37925	8.47
39.5627	94.71	0.1476	2.27797	9.92
40.2454	175.97	0.1476	2.24089	18.43
40.8272	162.16	0.1968	2.21029	16.98
44.1520	41.16	0.2952	2.05126	4.31
48.0675	54.88	0.2460	1.89292	5.75
49.3884	21.39	0.3936	1.84534	2.24
50.5721	91.44	0.1968	1.80489	9.57
55.6700	12.98	1.5744	1.65109	1.36

1120 and 740 cm^{-1}, respectively. The band at 645 cm^{-1} indicates the presence of inorganic species (Br) in the title compound. The assigned functional groups are presented in Table 3. The results confirm that 2A5NPBr compound has been formed.

3.3 UV–Vis–NIR analysis

The optical transparency of 2A5NPBr single crystal was studied by Perkin–Elmer Lambda-35 UV–Vis–NIR spectrophotometer in the scanning range of 200–1100 nm with slit width 1 nm. The transmittance and absorption spectra of 2A5NPBr are shown in Figs. 6 and 7, respectively. The grown crystal shows high transmittance in the visible and NIR region. The UV cut-off wavelength of the grown crystal was found to be 408 nm. The absorption is due to the
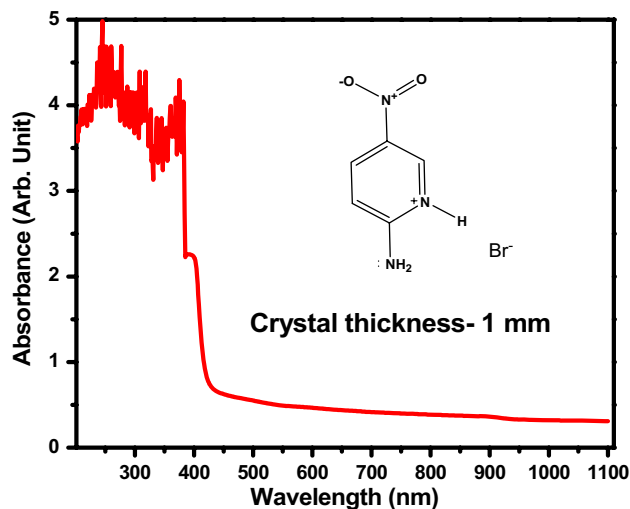
Table 3 FTIR wavenumbers and their assignments of 2A5NPBr

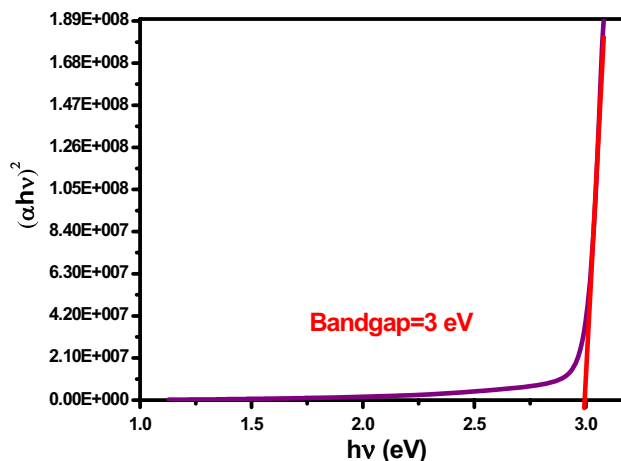| Wavenumber (cm^{-1})	Assignment
3324	ν_{as} (NH$_2$)
1665	ν_{as} (C=N)
1615	δ (N–H)
1520	ν (N–O)
1345	ν_{as} (N–O)
1120	C–H in-plane bending
740	C–H out-plane bending
645	N–H–Br rocking curve

where, ν_{as} is the asymmetric stretching, ν is the symmetric stretching and δ is the bending vibrations
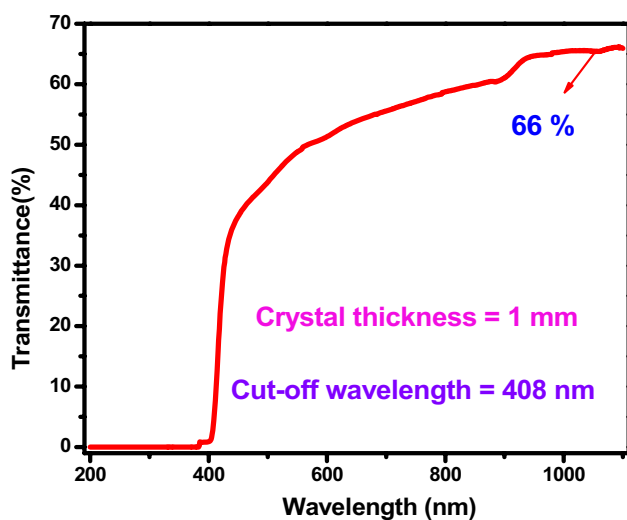
Fig. 6 UV–Vis–NIR transmission spectrum

Fig. 7 UV–Vis–NIR absorption spectrum

Fig. 8 Graph of $(\alpha\upsilon)^2$ versus photon energy (hυ) for 2A5NPBr single crystal

π–π* transition in the present molecule [12]. The value of absorption coefficient was calculated using the following expression:

$$\alpha = \frac{2.3026 \times \log_{10}\left(\frac{100}{T}\right)}{t} \tag{1}$$

where T is the transmittance (%) and t is the thickness of the sample (1 mm). The absorption coefficient was used to find out the bandgap (E_g) of the grown crystal. The optical bandgap of the grown crystal has been calculated by the Tauc's plot relation [13]:

$$(\alpha h\gamma) = A\left(h\gamma - E_g\right)^{\frac{1}{2}} \tag{2}$$

where A is constant, E_g is the band-gap energy, γ is the frequency of incident light, and h is the Planck's constant. The graph was plotted between photon energy (hγ) and $(\alpha h\gamma)^2$ by extrapolating the linear portion of the curve to zero absorption, as shown in Fig. 8. The optical bandgap (E_g) of 2A5NPBr crystal was found to be 3 eV. According to Planck–Einstein relation, the energy of a photon (E) is proportional to its frequency, and hence, theoretically, the optical band-gap energy of 2A5NPBr crystal can be calculated using the following relation:

$$E_g = \frac{hc}{\lambda} \tag{3}$$

where λ is the lower cut-off wavelength (408 nm). The bandgap of the grown 2A5NPBr crystal is found to be 3.03 eV, which is in good agreement with the value obtained from Fig. 8. When the light encounters a material, it can interact in different ways such as absorption, transmission, reflection, and scattering. The structural defects of the grown crystal are most

responsible for the optical transmission. In this case, the grown crystal possesses 66% of transmission in the near IR region, which makes the material favorable for NLO device applications. Although this crystal has lower cut-off wavelength at 408 nm with good transparency, it is still better than several organic/inorganic NLO crystals [14–20] which are presented in Table 4.

3.4 Chemical etching analysis

The surface feature of the grown 2A5NPBr crystal was identified by chemical etching analysis using COSLAB Model CMM-23 optical microscope in the reflection mode. The grown crystal must possess high quality for practical device applications, because the defects generated during growth cause the reduction of the NLO efficiency [21]. Hence, it is necessary to analyze the presence of microstructural imperfections in the grown crystals. In the present investigation, the chemical etching analysis was carried out using DMSO as an etchant at room temperature with the different time durations. The chemical etching study was performed using the transparent 2A5NPBr single crystal and the as-grown crystal surface is shown in Fig. 9a. The etch pits are produced after the successive etching for 3 s and it is shown in Fig. 9b. Figure 9c–e shows the elongated well-defined etch pits after etching for 7, 10, and 13 s, respectively. Finally, the size of the etch pits enlarged and overlapped after the etching for 20 s and it is shown in Fig. 9f. The obtained etch pits have resulted from the internal structural symmetry of the grown crystal [22]. The calculated etch pit density (EPD) of the grown crystal is 1.7×10^4 cm^{-2} for etching for 10 s. The less number of etch pit density (EPD) indicates that the grown crystal has more systematic packing of atoms/molecules. The etch pit density was calculated by the following relation:

$$\text{Density of etch pits } = \text{ Number of etch pits/Area.} \quad (4)$$

**Table 4** Comparative optical studies of 2A5NPBr and other NLO single crystals

Crystal name	Cut-off wavelength (nm)	References
2A5NPBr	408	Present work
2A5NPDP	450	[14]
LHPP	450	[15]
LAPP	496	[16]
NPNa	500	[17]
DAPNP	501	[18]
DMSI	510	[19]
HMSB	580	[20]

3.5 Photoconductivity studies

The grown crystal was subjected to photoconductivity measurement using Keithley pico-ammeter (MODELM6487) at room temperature. The good quality sample was selected for measurement and the electrical contacts were made on the crystal surface with 3 mm of distance using silver paste. Then, the sample was mounted inside a cryostat, which was evacuated to about 10^{-6} m bar. Two electrodes were connected to the DC power supply and their potential varied from 1 to 50 V with step voltage 1 V/s for the entire experiment. The dark current (i_d) was recorded by keeping the sample unexposed to any light radiation with their respective applied voltage (V). The photocurrent (i_p) was measured under the illumination of light radiation (Halogen source of 50 W) for the corresponding applied voltage. The plot of photocurrent and dark current as a function of applied voltage is shown in Fig. 10. From the figure, it can be seen that the photocurrent is higher than the dark current at every applied voltage, which defines the positive photoconductivity property of the title crystal. This phenomenon is due to the generation of charge carriers or their lifetime increases with the illumination of light radiation [23]. When the grown crystal is excited with photons of energy $E > E_g$ (E_g is the band-gap energy of the grown crystal), electron–hole pairs are generated and the conductivity of the sample increases [24]. As the grown crystal possesses high bandgap (E_g) for light absorption, it can be utilized towards the soliton wave communication, because the optical pulses propagate within the photonic bandgap for large distances without any distortion [25]. The positive photoconducting samples play a vital role in the photodetecting sensors and infrared (IR)-based photonic devices [23].

3.6 Thermal analysis

The thermal property of 2A5NPBr crystal was analyzed by TG-DTA analysis using Perkin–Elmer Diamond TG-DTA instrument in the temperature range 30–320 °C. The experiment was carried out at the heating rate of 10 °C per min in nitrogen atmosphere. The TG and DTA graph of 2A5NPBr is shown in Fig. 11. It is observed that there is no weight loss up to 175 °C. The TG curve reveals the three stages of decomposition in the title compound. The initial decomposition occurs in the temperature range between 175 and 210 °C with the mass loss of 57.5% which is due to the formation of volatile products such as HBr and NO_2. The second stage weight loss occurs in the temperature range between 210 and 255 °C with the weight loss of 19.5% which is due to the elimination of NH_3 and CN groups. The third stage weight loss is about 17.5% which is due to the elimination of hydrocarbons. The 5.5% of the weight was remaining in the platinum (Pt) crucible which is the residual
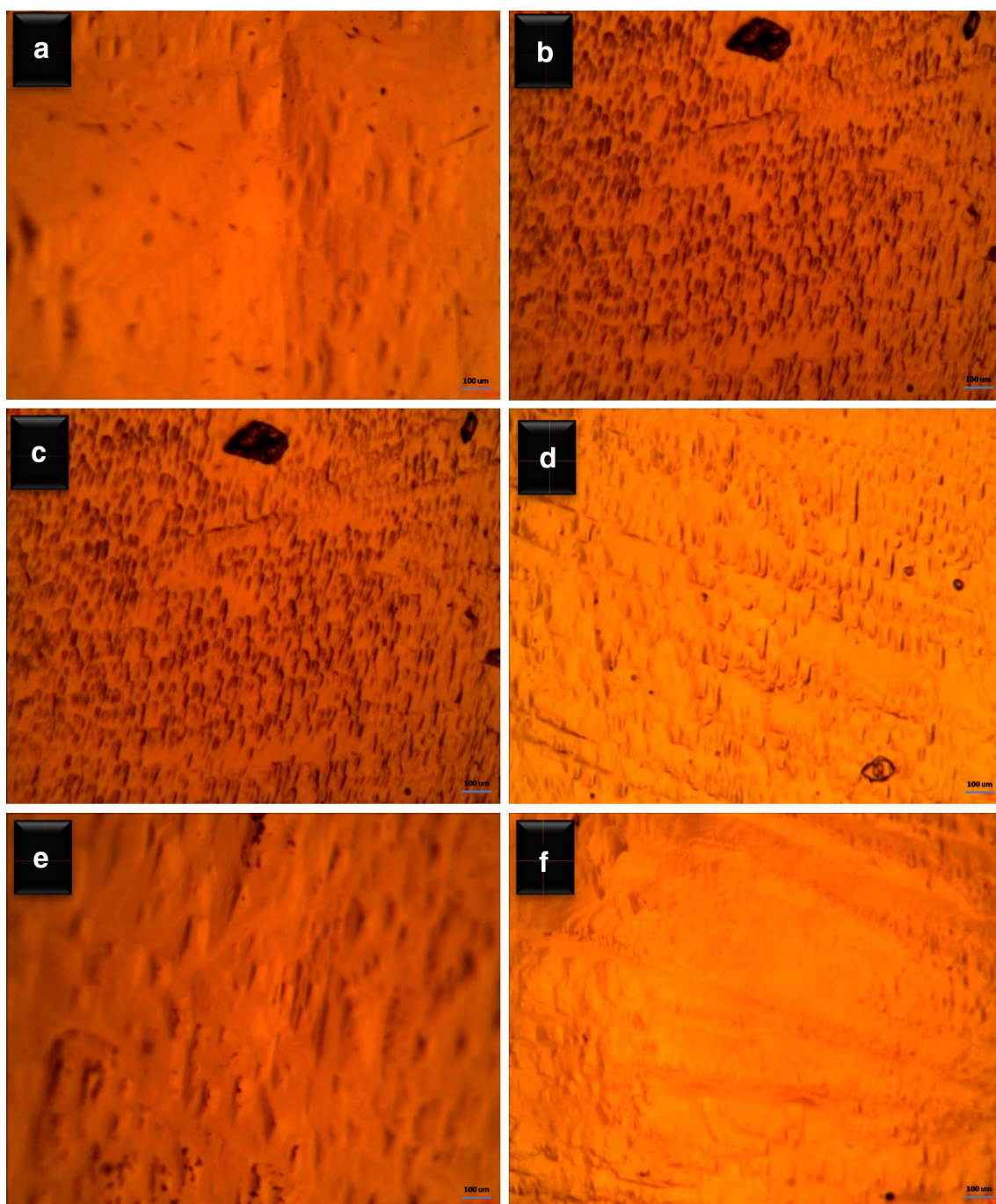
Fig. 9 **a** As grown 2A5NPBr crystal surface before etching. **b** Etch pits were initiated after the etching for 3 s. **c–e** Elongated rectangular shaped etch pits obtained after etching for 7, 10, and 13 s, respectively. **f** Etch pits were overlapped and some pits disappeared after the etching for 20 s

carbon. The decomposition of the grown crystal was compared with the theoretical and experimental values and it is listed in Table 5. From the DTA curve, the exothermic peak was observed at 210 °C, which indicates the decomposition point of the grown crystal and this peak coincides with the initial stage weight loss in the TG curve. On further heating, there is no significant change in DTA curve, which indicates

the remaining residual carbons. The title compound withstands the temperature up to 175 °C without any weight loss and it can be useful for any applications up to this temperature. In general, the bonding forces within the molecules are stronger than the lattice forces. The good thermal property is due to the stronger bonding forces between pyridine and the subsequent entry of Br^- anion in the crystal lattice.
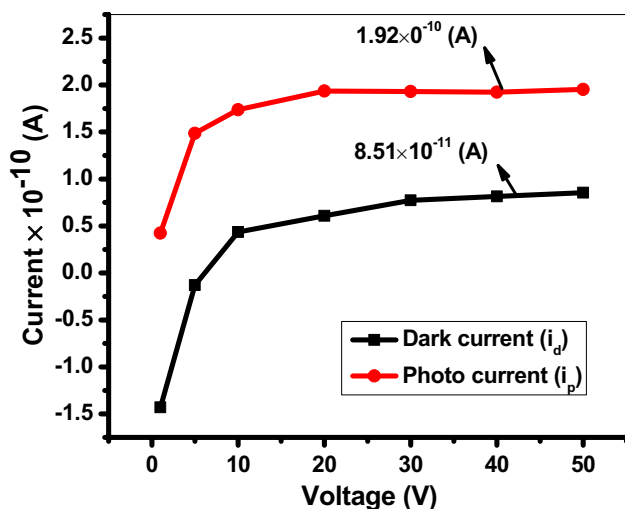
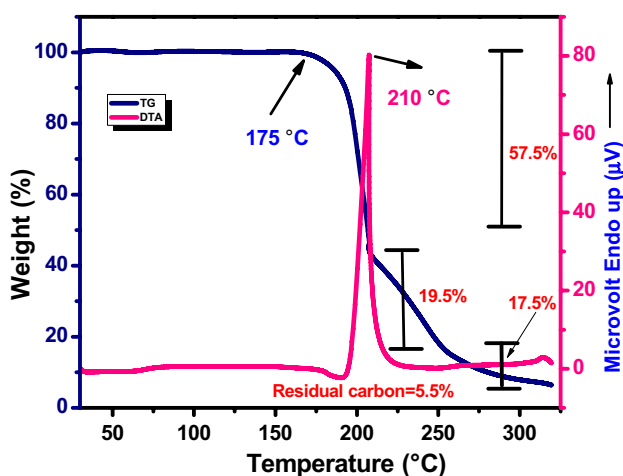**Fig. 10** Photoconductivity analysis for 2A5NPBr single crystal

Fig. 11 Thermal analysis for 2A5NPBr single crystal

3.7 Dielectric study

The dielectric study is one of the important characterizations to know the electrical response, lattice dynamics, and quality of the material. Hence, the dielectric constant and the dielectric loss of the grown 2A5NPBr crystal were studied using

PSM 1735 LCR instrument as a function of frequency from 100 Hz to 1 MHz. The cut and polished 2A5NPBr single-crystal samples were used for dielectric analysis. The silver coating was applied on the opposite faces of the sample and it gives good ohmic contact to both electrodes without any short circuit condition. The sample was placed between two copper electrodes, which acts as a parallel plate capacitor. The dielectric constant of the crystal was calculated using the equation:

$$\varepsilon' = \frac{C_p d}{\varepsilon_0 A} \tag{5}$$

where A is the area of cross section, d is the thickness of the sample, and ε_0 is the permittivity of free space (8.854×10^{-12} F/m). The dielectric constant as a function of frequency is shown in Fig. 12. Normally, the dielectric constant is high at lower frequency and it can be attributed to the contributions of electronic, ionic, orientation, and space charge polarizations [26]. It is observed that as the frequency increases, the dielectric constant of the grown crystal decreases. It is due to the improper period of motion of ions and molecules. The electronic polarizability only is active at a higher frequency and other polarizations are inactive. The dielectric loss of the grown crystal is shown in Fig. 13. The low value of dielectric loss indicates that the grown crystal possesses lesser defects with high quality.

3.8 Polarizability (α) of 2A5NPBr crystal

The electronic polarizability (α) is the significant factor for the desired effect of optical nonlinearity. There are many theoretical approaches available to calculate the electronic polarizability of molecule such as Penn analysis, Clausius–Mossotti relation, Lorentz–Lorenz equation, optical bandgap, and coupled dipole method (CDM). The electronic polarizability (α) of 2A5NPBr was calculated using dielectric constant at higher frequency ($\varepsilon' = 237$ at 1 MHz). The electronic polarization is strongly active in the higher frequency region. The density of 2A5NPBr is calculated by the following equation:

$$\rho = \frac{MZ}{N_A V} \tag{6}$$

Table 5 Thermal behavior of 2A5NPBr crystal as the function of temperature

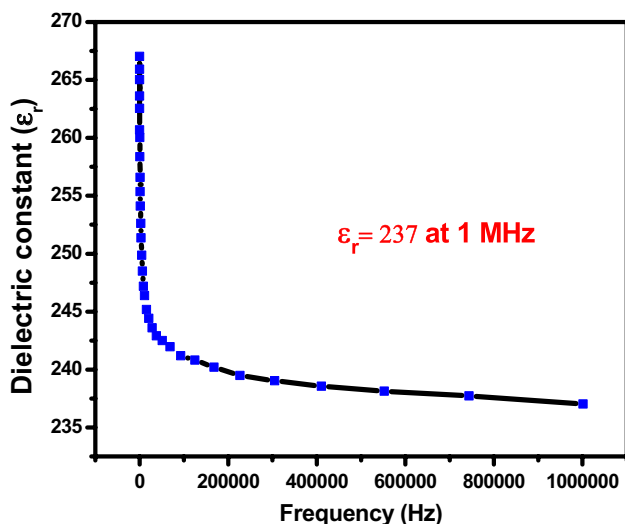| Compound name	Theoretical values (%)	Experimental values (%)	Temperature range (°C)
Mixture of gaseous products such as HBr and NO$_2$	57.6	57.5	175–210
Mixture of gaseous products such as NH$_3$ and CN	19.5	19.5	210–255
Hydrocarbons	17.3	17.5	255–320
Remaining residual carbons	5.4	5.5	Above 320

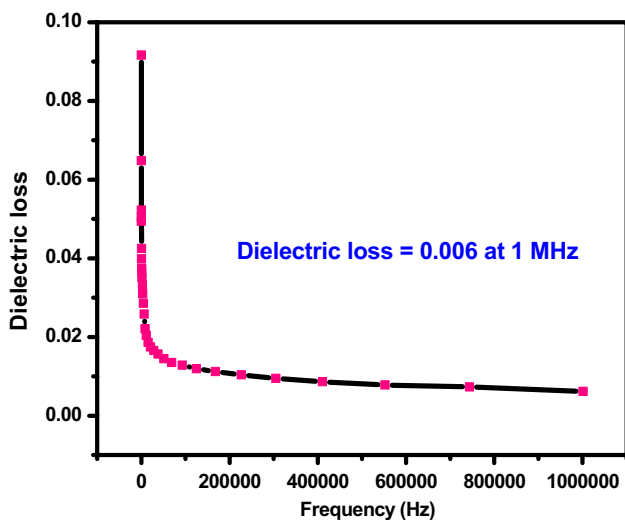**Fig. 12** Dielectric constant as a function of frequency (Hz)

Fig. 13 Dielectric loss as a function of frequency (Hz)

where M is the molecular weight of the grown crystal ($M = 220.03$ g/mol), Z is the number of molecules per unit cell ($Z = 2$), N_A is Avogadro's number (6.023×10^{23}), and V is the volume of unit cell ($V = 770.1$ Å^3). The calculated density of 2A5NPBr crystal is 1.887 g/cm^3. The valence electron plasma energy ($\hbar\omega_p$) is given by [27]:

$$\hbar\omega_p = 28.8 \left(\frac{Z' \times \rho}{M} \right)^{\frac{1}{2}} \tag{7}$$

where Z' is the total number of valence electrons of the title crystal ($C_5H_6O_2N_3Br$) and $Z' = ((5 \times Z'_C) + (6 \times Z'_H) + (2 \times Z'_O) + (3 \times Z'_N) + (1 \times Z'_{Br})) = 60$. It can be

calculated by substituting for each atom of C, H, N, O, and Br as corresponding valence electrons are 4, 1, 5, 6, and 7, respectively. According to the Penn model [28], the average Penn gap (E_P) and Fermi energy (E_F) [29] of 2A5NPBr were calculated using the following two relations:

$$E_P = \frac{\hbar\omega_p}{(\varepsilon' - 1)^{\frac{1}{2}}}, \tag{8}$$

$$E_F = 0.2948 (\hbar\omega_p)^{\frac{4}{3}}. \tag{9}$$

We can calculate the electronic polarizability (α) of the 2A5NPBr crystal using the relation:

$$\alpha = \left[\frac{(\hbar\omega_p)^2 S_0}{(\hbar\omega_p)^2 S_0 + 3E_P^2} \right] \times \frac{M}{\rho} \times 0.396 \times 10^{-24} \text{cm}^3 \tag{10}$$

where S_0 is a constant for a particular material which is given by

$$S_0 = 1 - \left[\frac{E_P}{4E_F} \right] + \frac{1}{3} \left[\frac{E_P}{4E_F} \right]^2. \tag{11}$$

The value of electronic polarizability (α) is also confirmed by the Clausius–Mossotti relation [30]:

$$\alpha = \frac{3M}{4\pi N_A \rho} \left(\frac{\varepsilon' - 1}{\varepsilon' + 2} \right). \tag{12}$$

According to Maxwell relation, the dielectric permittivity (ε') is equal to the square of refractive index, $\varepsilon' = n_0^2$. The linear refractive index (n_0) of the grown crystal has been found using Metricon Model 2010/M Prism coupler instrument with the laser wavelength of 632 nm. The n_0 value was found to be 1.527. The relationship between the electronic polarizability (α) and refractive index (n_0) in such fields can be described by the Lorentz–Lorenz equation [31] given by

$$\alpha = \frac{3M}{4\pi N_A \rho} \left(\frac{n_0^2 - 1}{n_0^2 + 2} \right). \tag{13}$$

The value of electronic polarizability (α) can also be obtained using optical bandgap, which is given by

$$\alpha = \left[1 - \frac{\sqrt{E_g}}{4.06} \right] \times \frac{M}{\rho} \times 0.396 \times 10^{-24} \text{cm}^3 \tag{14}$$

where E_g is the optical bandgap of 2A5NPBr crystal, which was calculated by the Touc's plot method. Electronic polarizability can be calculated based on coupled dipole method (CDM), which was introduced by Renne

and Nijboer [32, 33]. The atoms have no permanent electric dipole moment, but their dipole moments are induced by the local electric field, so that if the electron is at a nonzero distance from the nucleus, the atom is effectively an induced electric dipole. Therefore, the electronic polarizability (α) of 2A5NPBr crystal can be calculated by the following relation:

$$\alpha = \frac{Z'e^2}{m_e \omega_0^2} \tag{15}$$

where Z' is the total number of valence electrons, e is the charge of electron (1.602×10^{-19} C), m_e is the mass of electron (9.1×10^{-28} g), and ω_0 is the natural frequency ($2\pi f_0$), f_0 is 1 MHz. The obtained results are comparable to KDP and some other NLO crystals [34–37] and it is listed in Table 6.

3.9 Laser damage threshold studies

It is necessary to investigate the laser damage threshold analysis for nonlinear optical single crystals, because the crystals should have the ability to withstand high power lasers [38]. The laser damage threshold analysis was performed using a Q-switched Nd:YAG (1064 nm radiation) laser of 10 ns pulsewidth and 10 Hz repetition rate in transverse TEM_{00} mode. The observed LDT pattern of 2A5NPBr crystal is shown in Fig. 14. In general, the surface damage threshold is affected by the energy absorbing defects such as polishing contaminants and surface scratches, which get incorporated during mechanical polishing [5]. The present study was carried out using the polished flat single crystal, thus minimizing the surface defects and incorporated impurities. The surface damage of the grown crystal can be determined by the visual formation of damage or audible cracking and the
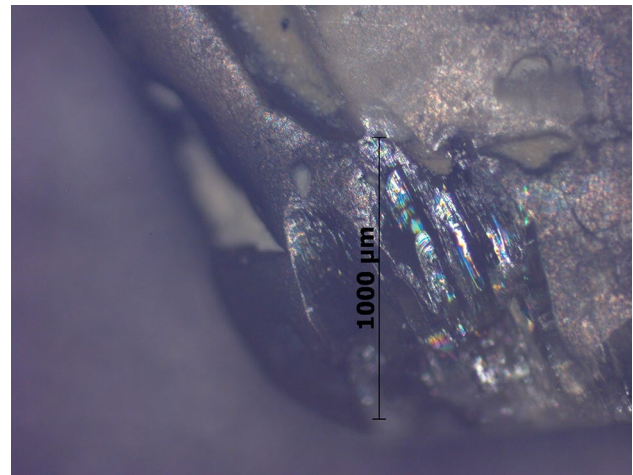

Fig. 14 Laser damaged pattern of 2A5NPBr single crystal

corresponding laser energy density was recorded by a power meter (Model: EPM-2000). The laser damage threshold of the grown crystal was evaluated by the following relation:

$$\text{Power density (Pd)} = \frac{E}{\tau \pi r^2} \tag{16}$$

where E is the input energy density (mJ), τ is the pulsewidth (ns), and r is the radius of the circular beam. The laser damage threshold of the grown crystal depends on several factors such as quality of crystal surface, density of crystal defects, wavelength of the laser beam, pulsewidth, repetition rate, laser intensity, location of the beam, longitudinal and transverse mode structures, laser beam size, and so on [39]. The mechanism for the laser damage threshold in the crystal is often very complex involving various processes

Table 6 Comparative polarizability analysis for 2A5NPBr and some other known NLO single crystals

Parameters	KDNP single crystal [34]	HSPI single crystal [35]	2A5NPBr single crystal (present work)	CDO single crystal [36]	KDP single crystal [37]
Plasma energy $\hbar\omega_p$ (eV)	21.51	18.887	20.65	16.225	17.33
Penn gap E_p (eV)	1.685	3.950	1.344	1.748	2.39
Fermi energy E_f (eV)	17.642	14.248	16.711	12.109	12.02
Electronic polarizability (α) using Penn analysis (cm⁻³)	5.43×10^{-23}	7.586×10^{-23}	4.55×10^{-23}	3.61×10^{-23}	2.14×10^{-23}
Electronic polarizability (α) using Clausius–Mossotti equation (cm⁻³)	5.44×10^{-23}	7.66×10^{-23}	4.57×10^{-23}	3.62×10^{-23}	2.18×10^{-23}
Electronic polarizability (α) using refractive index method (cm⁻³)	2.14×10^{-23}	–	1.42×10^{-23}	–	–
Electronic polarizability (α) using optical bandgap (cm⁻³)	3.09×10^{-23}	–	2.65×10^{-23}	1.85×10^{-23}	–
Electronic polarizability (α) using CDM method (cm⁻³)	5.57×10^{-23}	–	4.29×10^{-23}	–	–

Table 7 Comparison of laser-induced damage threshold (LDT) for 2A5NPBr and some other known NLO crystals

Crystal name	Wavelength (nm)	Pulsewidth (ns)	Laser damage threshold (GW/cm^2)	References
KB5	1064	12	> 0.08	[40]
LBO	1064	18	> 0.6	[40]
LFMH	1064	11	1.5	[40]
KTP	1064	11	> 1.5–2.2	[40]
L-Serine	1064	20	2.1	[41]
Benzamidazole	1064	20	2.86	[42]
2A5NPBr	1064	10	3.4	Present work
L-Alaninium maleate	–	–	4.9	[43]
KDP	1064	1	5	[44]

such as multi-photon absorption, electron avalanche effect, photochemical dissociation, photoionization by thermal absorption, electrostrictive fracture, etc [4]. Hence, the thermal effect plays an important role in laser damage threshold, which causes melting or decomposition with the exposure of high power lasers. From this study, it is observed that the laser damage threshold (LDT) depends on the nature of the grown crystal and experimental parameters. From the experiment, the value of laser damage threshold of 2A5NPBr was found to be 3.4 GW/cm^2, which is higher than several NLO single crystals [40–44] and it is presented in Table 7.

4 Z-scan technique

Z-scan technique is a reliable method for determining the nonlinear optical properties of materials (i.e., nonlinear absorption and nonlinear refraction). The method has been developed for wide ranging applications such as optical limiting [45] multi-photon polymerization [46] as well as optical switching [47]. The Z-scan method was developed by Stryland and Sheik-Bahae [45, 48]. In this experiment, the third-order NLO properties of 2A5NPBr crystal were investigated using He–Ne laser (5 mW) of wavelength 632.8 nm and the beam diameter 0.5 mm. The laser was focused with a Gaussian filter to convert input laser beam into Gaussian form. The TEM$_{00}$ mode was used to polarize the optical beam with the focal length 30 mm. The waist beam (ω_o) was 12.05 μm. The thickness of the sample used was 0.6 mm and it was fixed on a holder at 90° with respect to the laser beam. The sample was moved along the negative (– Z) to positive (+Z) axis with the propagation direction of the laser beam. The output intensity of a laser beam directly depends on the refractive index of the materials and its absorption nature. The obtained open and closed aperture spectra of 2A5NPBr crystal are shown in Figs. 15 and 16, respectively. The sample causes an additional focusing or defocusing, depending on the nonlinear refraction values. The maximum transmission at the focus ($Z=0$) indicates the saturation of absorption (SA) and minimum transmittance reveals
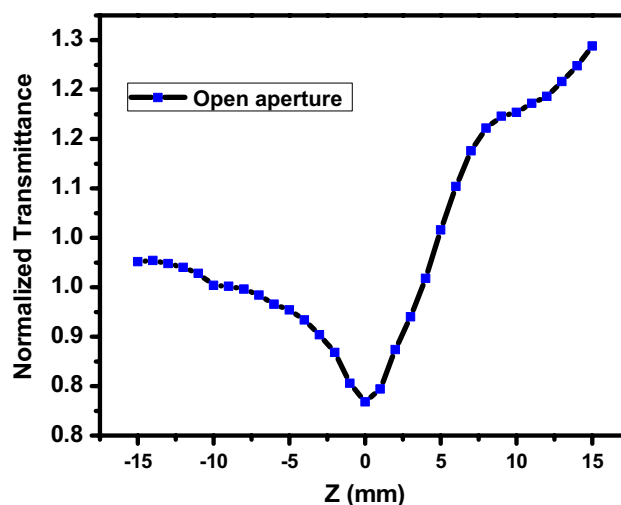

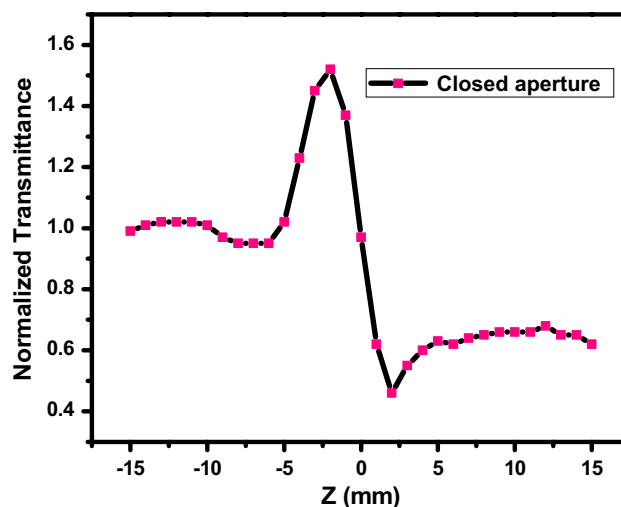**Fig. 15** Open aperture spectrum of 2A5NPBr single crystal

Fig. 16 Closed aperture spectrum of 2A5NPBr single crystal

the reverse saturation absorption (RSA) and two/multi-photon absorption.

The nonlinear refractive index of 2A5NPBr crystal was calculated using the difference between the transmittance of peak and valley (ΔT_{p-v}) and it can be written in terms of axis phase shift at the focus:

$$|\Delta \varphi| = \frac{\Delta T_{p-v}}{0.406(1-S)^{0.25}} \tag{17}$$

where $\Delta \varphi$ is the axis phase shift at the focus, and S is the linear transmittance aperture and it can be calculated using the relation [49]:

$$S = 1 - \exp\left(\frac{-2r_a^2}{\omega_a^2}\right) \tag{18}$$

where r_a is the radius of aperture (0.2 mm) and ω_a is the beam radius at the aperture. From the closed aperture experiment, the nonlinear refractive index (n_2) of the grown 2A5NPBr crystal was calculated using the relation:

$$n_2 = \frac{\Delta \phi}{kI_0 L_{eff}} \left(m^2/W\right). \tag{19}$$

The nonlinear absorption coefficient (β) can be determined using open aperture spectrum. The value of β will be positive for two-photon absorptions or reverse saturable absorption and negative for saturable absorption [48]. β was calculated using the following equation:

$$\beta = \frac{2\sqrt{2}\Delta T}{I_0 L_{eff}} \left(m/W\right) \tag{20}$$

where k is the wave number ($k = 2\pi/\lambda$), ΔT is peak value at the open aperture, and I_0 is the intensity of the laser at the focus (25 MW/m^2). The effective thickness (L_{eff}) of the sample can be calculated using the expression:

$$L_{eff} = \frac{1 - \exp(-\alpha L)}{\alpha} \tag{21}$$

where α is the linear absorption coefficient and L is the thickness of the sample. The real and imaginary parts of the third-order nonlinear optical susceptibility ($\chi^{(3)}$) were estimated using the relations:

$$R_e\chi^{(3)} \ (esu) = \frac{10^{-4}\varepsilon_0 c^2 n_0^2 n_2}{\pi} \left(cm^2/W\right) \tag{22}$$

$$I_m\chi^{(3)} \ (esu) = \frac{10^{-2}\varepsilon_0 c^2 n_0^2 \lambda\beta}{4\pi^2} \left(cm/W\right) \tag{23}$$

where ε_0 is the vacuum permittivity (8.854×10^{-12} F/m), c is the velocity of light in vacuum, n_0 is the linear refractive index of the sample, and λ is the wavelength of laser beam. The third order nonlinear optical susceptibility ($\chi^{(3)}$) of the 2A5NPBr crystal can be calculated using the following expression:

$$\chi^{(3)} = \sqrt{\left(R_e\chi^{(3)}\right)^2 + \left(I_m\chi^{(3)}\right)^2}. \tag{24}$$

In addition, the second-order molecular hyperpolarizability (γ) of the grown crystal is related to the third-order bulk susceptibility and it is calculated by the following equation [50]:

$$\gamma = \frac{\chi^{(3)}}{N * f^4} \tag{25}$$

where N^* is the number of molecules per cm^3 and f is the local-field correction factor. The value of N^* can be calculated by the following equation:

$$N *= \frac{\rho N_A}{M} \tag{26}$$

where N^* was found to be 5.60×10^{21} cm^3. According to Lorentz equation, the local-field correction factor can be calculated by the following equation:

$$f = \frac{\left(n_0^2 + 2\right)}{3}. \tag{27}$$

The calculated value of third-order nonlinear refractive index (n_2) (from closed aperture) is 2.48×10^{-11} m^2/W, third-order nonlinear absorption coefficient (β) (from open aperture) is 3.399×10^{-5} m/W, absolute third-order nonlinear susceptibility ($\chi^{(3)}$) is 6.76×10^{-9} esu, and the obtained second-order molecular hyperpolarizability (γ) is 2.83×10^{-31} esu for 2A5NPBr crystal. The experimental details and the obtained results are presented in Table 8. The third-order susceptibility is found to be larger than the other NLO crystals [51–57], as shown in Table 9. The large value of ($\chi^{(3)}$) can be attributed to the electron density transfer (donor to acceptor) within the 2A5NPBr molecular system. The negative sign of the nonlinear refractive index (n_2) indicates the self-defocusing nature of the material. This may have an advantage in practical devices, by providing a self-protecting mechanism for the limiter in optical systems such as direct viewing devices (telescopes, gun sights, etc.) and night vision devices [58].

5 Conclusions

Good quality, semi-organic nonlinear optical 2A5NPBr single crystals were grown by slow evaporation solution technique (SEST) with the growth period of 60 days. The centric nature and unit cell parameters of the grown crystal were

Table 8 Parameters measured in Z-scan measurement for 2A5NPBr single crystals

Third-order NLO parameters	Obtained values
Laser wavelength (λ)	632.8 nm
Lens focal length (f)	30 mm
Optical path length	850 mm
Beam radius of the aperture (ω_a)	3.3 mm
Aperture radius (r_a)	2 mm
Sample thickness (L)	0.6 mm
Effective thickness (L_{eff})	0.499 mm
Linear transmittance aperture (S)	0.52
Linear absorption coefficient (α)	632.54
Linear refractive index (n_o)	1.5274
Nonlinear refractive index (n_2)	$2.48 \times 10^{-11} \frac{m^2}{W}$
Nonlinear absorption coefficient (β)	$3.39 \times 10^{-5} \frac{m^2}{W}$
Real part of third-order susceptibility (Re ($\chi^{(3)}$))	1.45×10^{-09} esu
Imaginary part of third-order susceptibility (Im ($\chi^{(3)}$))	6.6×10^{-09} esu
Third-order nonlinear optical susceptibility ($\chi^{(3)}$)	6.76×10^{-09} esu
Second-order molecular hyperpolarizability (γ)	2.83×10^{-31} esu

Table 9 Comparison of ($\chi^{(3)}$) value of 2A5NPBr and some other NLO single crystals

Crystal name	Wavelength (λ) nm	Third-order nonlinear susceptibility ($\chi^{(3)}$) esu	References
2ADPTS	632.8	3.143×10^{-4}	[51]
2M6NQE	632.8	1.469×10^{-5}	[52]
4DMAPPTS	532	1.476×10^{-6}	[53]
KDC	532	4.68×10^{-6}	[54]
2A5NPBr	632.8	6.76×10^{-09}	Present work
AAP	532	6.2×10^{-9}	[55]
VMST	632.8	9.6×10^{-12}	[56]
KBBT	–	0.99×10^{-13}	[57]
KDP	532	4.02×10^{-14}	[59]

confirmed by single-crystal XRD analysis. The FTIR analysis reveals the formation of 2A5NPBr compound. The grown crystal shows 66% optical transmittance in visible and NIR region and it indicates its usefulness for nonlinear optical applications. The etch pit density of the grown crystal was found to be 1.7×10^4 cm^{-2} by chemical etching analysis. The photoconductivity studies confirm that the grown 2A5NPBr crystal possesses positive photoconductivity nature. The grown crystal is thermally stable up to 175 °C which was confirmed by TG-DTA analysis. The dielectric measurement reveals that the grown crystal has normal dielectric behavior. The low value of dielectric loss evidences that the grown crystal possesses good quality. The electronic polarizability

(α) of 2A5NPBr was found to be larger than that of KDP single crystal. The grown crystal has larger laser damage threshold (3.4 GW/cm^2) compared to several NLO crystals, which is an essential requirement for the fabrication of NLO and high power laser devices. The third-order NLO parameters were evaluated and the results showed that the grown crystal exhibits good third-order nonlinear susceptibility. The Z-scan study reveals that the grown crystal has self-defocusing nature and reverse saturation absorption (RSA). The present results suggest that the grown crystal can be useful for optical limiting and photonic device applications.

References

1. L. Tutt, T. Boggess, A review of optical limiting mechanisms and devices using organics, fullerenes, semiconductors and other materials. Prog. Quantum Electron. **17**, 299–338 (1993)
2. DZ Chemla (Ed), Nonlinear optical properties of organic molecules and crystals, 1st edn., (Academic Press, Orlando, 1987)
3. C. Aakeröy, A. Beatty, M. Nieuwenhuyzen, M. Zou, A structural study of 2-amino-5-nitropyridine and 2-amino-3-nitropyridine: intermolecular forces and polymorphism. J. Mater. Chem. **8**, 1385–1389 (1998)
4. G. Anandha babu, P. Ramasamy, A. Chandramohan, Studies on the synthesis, structure, growth and physical properties of an organic NLO crystal: 2-amino-5-nitropyridinium phenolsulfonate. Mater. Res. Bull. **46**, 2247–2251 (2011)
5. G. Anandha Babu, P. Ramasamy, J. Philip, Studies on the growth and physical properties of nonlinear optical crystal: 2-amino-5-nitropyridinium-toluenesulfonate. Mater. Res. Bull. **46**, 631–634 (2011)
6. K. Senthil, S. Kalainathan, F. Hamada, Y. Kondo, Bulk crystal growth and nonlinear optical characterization of a stilbazolium derivative crystal: 4-[2-(3,4-dimethoxyphenyl)ethenyl]-l methylpyridinium tetraphenylborate (DSTPB) for NLO device fabrication. RSC Adv. **5**, 79298–79308 (2015)
7. X. Wang, H. Fang, Q. Ren, J. Sun, T. Li, G. Zhang et al., Preparation, spectrographic characterization, thermal, second and third order nonlinear optical properties of 4,5-bis(foroylsulfanyl)-1,3-dithiole-2-thione. Laser Phys. **19**, 1858–1866 (2009)
8. J. Pécaut, J. Lévy, R. Masse, Structural evidence in 2-amino-5-nitropyridinium halides (Cl–, Br–) of herringbone motifs favourable to efficient quadratic non-linear optical properties. J. Mater. Chem. **3**, 999–1003 (1993)
9. S. Dhanuskodi, A. Pricilla Jeyakumari, S. Manivannan, Semiorganic NLO material for short-wavelength generation 2-amino-5-nitropyridinium bromide. J. Cryst. Growth **282**, 72–78 (2005)
10. C. Indumathi, SAC Raj, Optical studies of polymorphic 2-amino-5-nitropyridinium bromide., Int. J. ChemTech Res., **6**, 1611–1613 ISSN: 0974–4290. (2014)
11. W. Kaminsky, From CIF to virtual morphology using the WinXMorphprogram. J. Appl. Crystallogr. **40**, 382–385 (2007)

12. A. Ibanez, J. Levy, C. Mouget, E. Prieur, Crystal growth of a promising nonlinear optical material: 2-amino-5-nitropyridinium chloride. J. Solid State Chem. **129**, 22–29 (1997)

13. J. Tauc, R. Grigorovici, A. Vancu, Optical properties and electronic structure of amorphous germanium. Phys. Status Solidi (B) **15**, 627–637 (1966)

14. A. Jeyakumari, S. Manivannan, S. Dhanuskodi, Spectral and optical studies of 2-amino-5-nitropyridinium dihydrogen phosphate: a semiorganic nonlinear optical material., Spectrochim. Acta Part A Mol. Biomol. Spectr., **67**, 83–86 (2017)

15. T. Chen, Z. Sun, C. Song, Y. Ge, J. Luo, W. Lin et al., Bulk crystal growth and optical and thermal properties of the nonlinear optical crystall-histidinium-4-nitrophenolate 4-nitrophenol (LHPP). Cryst. Growth Des. **12**, 2673–2678 (2012)

16. V. Sivasubramani, M. Anis, S. Hussaini, G. Muley, M. Senthil Pandian, P. Ramasamy, Bulk growth of organic non-linear optical (NLO) L-arginine 4-nitrophenolate 4-nitrophenol dihydrate (LAPP) single crystals by Sankaranarayanan–Ramasamy (SR) method. Mater. Res. Innov. **21**, 426–433 (2017)

17. M. Mahadevan, P. Anandan, K. Ramachandran, M. Arivanandhan, Y. Hayakawa, Studies on the growth aspects and characterization of sodium para-nitro phenolate single crystals for nonlinear optical applications. Optik Int. J. Light Electron Opt. **125**, 5515–5518 (2017)

18. T. Chen, Z. Sun, L. Li, S. Wang, Y. Wang, J. Luo et al., Growth and characterization of a nonlinear optical crystal-2,6-diamino-pyridinium 4-nitrophenolate 4-nitrophenol (DAPNP). J Cryst. Growth **338**, 157–161 (2012)

19. M. Kumar, S. Sudhahar, G. Bhagavannarayana, R. Kumar, Crystal growth, structural and optical properties of an organic ion-complex crystal: 4-*N,N*-dimethylamino-4′-*N*′-methylstilbazolium iodide. Optik Int. J. Light Electron Opt. **125**, 5641–5646 (2017)

20. A. Gill, S. Kalainathan, G. Bhagavannarayana, Organic nonlinear optical crystal 4-hydroxy-N-methyl 4-stilbazolium besylate synthesis and characterization. Mater. Lett. **64**, 1989–1991 (2017)

21. A. Senthil, P. Ramasamy, Investigation on the SR method growth, etching, birefringence, laser damage threshold and thermal characterization of strontium bis (hydrogen l-malate) hexahydrate single crystal. J. Cryst. Growth **401**, 200–204 (2014)

22. K Sangwal Etching of crystals: theory, experiment and application, 1st edn., (North Holland Physics Publishing, Amsterdam, 1987)

23. N Joshi Photoconductivity, 1st edn., (Marcel Dekker, New York, 1990)

24. RH Bube, Photoconductivity of solids, 1st edn., (Wiley Inter Science, New York, 1981)

25. B. Boaz, S. Navis Priya, J. Linet, P. Deva Prasath, S. Das, Photoconductivity and dielectric studies on NLO active NPNa and NPLi single crystals. Opt. Mater. **29**, 827–832 (2007)

26. D. Xue, K. Kitamura, Dielectric characterization of the defect concentration in lithium niobate single crystals. Solid State Commun. **122**, 537–541 (2002)

27. JD Jackson, Classical electrodynamics, 49th edn., P 321, (Wiley Eastern, New Delhi, 1978)

28. D. Penn, Wave-number-dependent dielectric function of semiconductors. Phys. Rev. **128**, 2093–2097 (1962)

29. C. Balarew, R. Duhlev, Application of the hard and soft acids and bases concept to explain ligand coordination in double salt structures. J. Solid State Chem. **55**, 1–6 (1984)

30. P.V. Rysselberghe, Remarks concerning the Clausius-Mossotti Law. J. Phys. Chem. **36**, 1152–1155 (1932)

31. M. Born, E. Wolf, 2nd edn., (Osnovy optiki, Moscow, 1973)

32. M. Renne, B. Nijboer, Microscopic derivation of macroscopic Van der Waals forces. Chem. Phys. Lett. **1**, 317–320 (1967)

33. B. Nijboer, M. Renne, Microscopic derivation of macroscopic van der waals forces. Chem. Phys. Lett. **2**, 35–38 (1968)

34. P. Karuppasamy, V. Sivasubramani, M. Pandian, P. Ramasamy, Growth and characterization of semi-organic third order nonlinear optical (NLO) potassium 3,5-dinitrobenzoate (KDNB) single crystals. RSC Adv. **6**, 109105–109123 (2016)

35. K. Nivetha, S. Kalainathan, M. Yamada, Y. Kondo, F. Hamada, Investigation on the growth, structural, HOMO–LUMO and optical studies of 1-ethyl-2-[2-(4-hydroxy-phenyl)-vinyl]-pyridinium iodide (HSPI)-a new stilbazolium derivative for third-order NLO applications. RSC Adv. **6**, 35977–35990 (2016)

36. K. Chauhan, S. Arora, Diamagnetic and photoabsorption characterisation of gel-grown cadmium oxalate single crystals. Cryst. Res. Technol. **44**, 189–196 (2009)

37. P. Vasudevan, S. Sankar, S. Gokul Raj, Studies on second harmonic generation efficiency of organic material l-arginine maleate dihydrate. Optik Int. J. Light Electron Opt. **124**, 4155–4158 (2013)

38. K. Senthil, S. Kalainathan, A. Kumar, P. Aravindan, Investigation of synthesis, crystal structure and third-order NLO properties of a new stilbazolium derivative crystal: a promising material for nonlinear optical devices. RSC Adv. **4**, 56112–56127 (2014)

39. N. Boling, M. Crisp, G. Dubé, Laser induced surface damage, Appl. Opt. **12**, 650–660 (1973)

40. D. Joseph Daniel, P. Ramasamy, Studies on semi-organic non linear optical single crystal: Lithium formate monohydrate ($HCO_2Li \cdot H_2O$). Opt. Mater. **36**, 971–976 (2014)

41. K. Rajesh, P. Kumar, Structural, Linear, and Nonlinear Optical and Mechanical Properties of New Organic L-Serine Crystal., J. Mater., 1–5 (2014) (2014)

42. N. Vijayan, G. Bhagavannarayana, R. Ramesh Babu, R. Gopalakrishnan, K. Maurya, P. Ramasamy, A comparative study on solution- and Bridgman-Grown single crystals of benzimidazole by high-resolution X-ray diffractometry, Fourier transform infrared, microhardness, laser damage threshold, and second-harmonic generation measurements. Cryst. Growth Des. **6**, 1542–1546 (2006)

43. S. Martin Britto Dhas, M. Suresh, G. Bhagavannarayana, S. Natarajan, Growth and characterization of l-Tartaric acid, an NLO material. J. Cryst. Growth **309**, 48–52 (2007)

44. X. Liu, X. Wang, X. Yin, S. Liu, W. He, L. Zhu et al., Bulk growth and physical properties of diguanidinium phosphate monohydrate (G2HP) as a multi-functional crystal. Crystengcomm **16**, 930–938 (2014)

45. E. Van Stryland, H. Vanherzeele, M. Woodall, M. Soileau, A. Smirl, S. Guha et al., Two photon absorption, nonlinear refraction, and optical limiting in semiconductors. Opt. Eng. **24**, 613–623 (1985)

46. C. Mendonca, D. Correa, F. Marlow, T. Voss, P. Tayalia, E. Mazur, Three-dimensional fabrication of optically active microstructures containing an electroluminescent polymer., Appl. Phys. Lett., **95**, 113309 (1–3) (2009)

47. K. DeLong, K. Rochford, G. Stegeman, Effect of two-photon absorption on all-optical guided-wave devices. Appl. Phys. Lett. **55**, 1822–1823 (2017)

48. M. Sheik-Bahae, A. Said, T. Wei, D. Hagan, E. Van Stryland, Sensitive measurement of optical nonlinearities using a single beam. IEEE J. Quantum Electron. **26**, 760–769 (1990)

49. S. Shettigar, G. Umesh, K. Chandrasekharan, B. Kalluraya, Third order nonlinear optical properties and two photon absorption in newly synthesized phenyl sydnone doped polymer. Synth. Met. **157**, 142–146 (2007)

50. M. Zhao, B. Singh, P. Prasad, A systematic study of polarizability and microscopic third-order optical nonlinearity in thiophene oligomers. J. Chem. Phys. **89**, 5535–5541 (1988)

51. R. Jauhar, S. Kalainathan, P. Murugakoothan, Three dimensional organic framework of 2-amino 4, 6 dimethoxypyrimidine

p-toluenesulfonic acid monohydrate: synthesis, single crystal growth and its properties. J. Cryst. Growth **424**, 42–48 (2015)

52. M. Nirosha, S. Kalainathan, S. Sarveswari, V. Vijayakumar, A. Srikanth, Growth, spectral, optical, thermal, surface analysis and third order nonlinear optical properties of an organic single crystal: 1-(2-Methyl-6-nitro-4-phenyl-3-quinolyl) ethanone, Spectrochim. Acta Part A Mol. Biomol. Spectr., 137, (2015) pp. 23–28

53. I. Bincy, R. Gopalakrishnan, Studies on synthesis, growth and characterization of a novel third order nonlinear optical 4-dimethylaminopyridinium p-Toluenesulfonate single crystal. Opt. Mater. **37**, 267–276 (2014)

54. T. Thilak, M. Ahamed, G. Vinitha, Third order nonlinear optical properties of potassium dichromate single crystals by Z-scan technique. Optik Int. J. Light Electron Opt. **124**, 4716–4720 (2013)

55. A. Arunkumar, P. Ramasamy, Bulk single crystals of ammonium acid phthalate grown by the Sankaranarayanan–Ramasamy method for optical limiting applications. J. Cryst. Growth **401**, 195–199 (2014)

56. M. Krishna Kumar, S. Sudhahar, P. Pandi, G. Bhagavannarayana, R. Mohan Kumar, Studies of the structural and third-order nonlinear optical properties of solution grown 4-hydroxy-3-methoxy-4′-N'-methylstilbazolium tosylate monohydrate crystals. Opt. Mater. **36**, 988–995 (2014)

57. F. Li, N. Zong, F. Zhang, J. Yang, F. Yang, Q. Peng et al., Investigation of third-order optical nonlinearity in $KBe_2BO_3F_2$ crystal by Z-scan. Appl. Phys. B **108**, 301–305 (2012)

58. Y. Zhou, E. Wang, J. Peng, J. Liu, C. Hu, R. Huang et al., Synthesis and the third-order optical nonlinearities of two novel charge-transfer complexes of a heteropoly blue type $(C_9H_7NO)_4$ $H_7PMo_{12}O_{40}\cdot3H_2O$ $(C_9H_7NO$ = quinolin-8-ol) and (phen)3 $H_7PMo_{12}O_{40}\cdot CH_3CN\cdot H._2O$ (phen = 1,10-phenanthroline), Polyhedron, 18,1419–1423 (1999)

59. D. Wang, T. Li, S. Wang, J. Wang, Z. Wang, X. Xu, F. Zhang, Study on nonlinear refractive properties of KDP and DKDP crystals. RSC Adv. **6**, 14490–14495 (2016)